Direct measurements of the coordination of lever arm swing and the catalytic cycle in myosin V

Darshan V. Trivedi[a], Joseph M. Muretta[b], Anja M. Swenson[a], Jonathon P. Davis[c], David D. Thomas[b], and Christopher M. Yengo[a,1]

[a]Department of Cellular and Molecular Physiology, College of Medicine, Pennsylvania State University, Hershey, PA 17033; [b]Department of Biochemistry, Molecular Biology, and Biophysics, School of Medicine, University of Minnesota, Minneapolis, MN 55455; and [c]Department of Physiology and Cell Biology, College of Medicine, The Ohio State University, Columbus, OH 43210

Edited by Thomas D. Pollard, Yale University, New Haven, CT, and approved October 15, 2015 (received for review September 4, 2015)

Myosins use a conserved structural mechanism to convert the energy from ATP hydrolysis into a large swing of the force-generating lever arm. The precise timing of the lever arm movement with respect to the steps in the actomyosin ATPase cycle has not been determined. We have developed a FRET system in myosin V that uses three donor–acceptor pairs to examine the kinetics of lever arm swing during the recovery and power stroke phases of the ATPase cycle. During the recovery stroke the lever arm swing is tightly coupled to priming the active site for ATP hydrolysis. The lever arm swing during the power stroke occurs in two steps, a fast step that occurs before phosphate release and a slow step that occurs before ADP release. Time-resolved FRET demonstrates a 20-Å change in distance between the pre- and postpower stroke states and shows that the lever arm is more dynamic in the post-power stroke state. Our results suggest myosin binding to actin in the ADP.Pi complex triggers a rapid power stroke that gates the release of phosphate, whereas a second slower power stroke may be important for mediating strain sensitivity.

myosin | actin | FRET | force generation | kinetics

Myosins are molecular machines that use the energy from ATP hydrolysis to generate force and motion through a cyclic interaction with actin filaments. Actomyosin-based force generation is used to drive muscle contraction, organelle transport, cytokinesis, membrane tension generation, and numerous biological tasks (1). Most myosins display a conserved structural fold and ATPase mechanism, suggesting the mechanism of energy transduction is similar in the myosin superfamily. A long α-helix which extends from the motor core binds a variable number of light chains and is referred to as the "lever arm" (2). A relative sliding motion of myosin (thick) and actin (thin) filaments in muscle forms the basis of the cross-bridge hypothesis which provides a more general view of the mechanism of muscle contraction (3). The swinging lever arm hypothesis provides a more molecular basis of muscle contraction. In this hypothesis, the lever arm swing is associated with the actin-activated product release steps, in turn leading to force generation by the attached cross-bridge (4). However, the precise timing of the lever arm swing and product release steps has remained a central question since early studies of actomyosin (5).

Scheme I represents a simplified actomyosin ATPase cycle that can be used to describe the kinetics of key steps in the catalytic cycle (5, 6). The weak actin-binding states of myosin are indicated in bold, and the actin-bound biochemical transitions are indicated by equilibrium constants with a prime. ATP binding to myosin occurs in two steps, an initial collision complex (K'_1) followed by a structural change that is associated with a weak actin-binding conformation (open actin-binding cleft) and high affinity for ATP (closed nucleotide-binding pocket) (K'_2). The movement of the lever arm into the prepower stroke state is thought to occur during one of the ATP-binding steps and before ATP hydrolysis. The ATP hydrolysis step (K_3) occurs while myosin remains in a weak actin-binding conformation. When myosin binds to actin with the hydrolyzed products in the active site, there is a dramatic acceleration of the product release steps, first phosphate (Pi) (K'_4) and then ADP (K'_5). It is during the actin-activated product release steps that the lever shifts from a pre- to a postpower stroke state and force generation occurs. In addition, myosin shifts from a weak to a strong actin-binding conformation as a result of actin-induced closure of the actin-binding cleft. Thus, to determine the structural mechanism of actomyosin-based force generation, it is crucial to design a method of measuring the position of the lever arm during the formation of the prepower stroke state (recovery stroke) as well as during the transition from the pre- to postpower stroke states (power stroke).

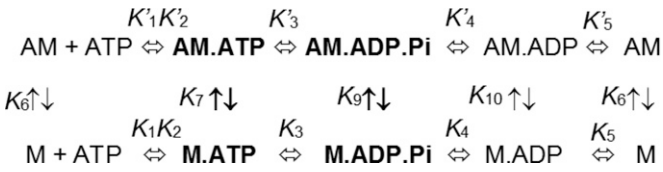

Scheme 1. The actomyosin ATPase cycle.

In the current study we engineered myosin V (MV), a motor that is well characterized both kinetically and structurally, to contain three site-specific donor–acceptor pairs that allowed us to measure the lever arm swing directly by FRET. We provide direct evidence that the lever arm swings into the prepower stroke state (recovery stroke) when the active site is primed for ATP hydrolysis. The force-generating swing (the power stroke)

Significance

Myosins interact with actin filaments and convert the chemical energy from ATP hydrolysis into mechanical work. The swinging lever arm hypothesis describes the molecular mechanism of actomyosin-based force generation that is essential for cell motility, muscle contraction, and cell division. In this model the light chain-binding region of myosin undergoes a major conformational change, which drives force generation. However, the temporal kinetics of structural changes in the lever arm in relation to the product release steps of the catalytic cycle are not well established. By using a FRET-based strategy, we demonstrate the lever arm swing occurs in two steps, a rapid step prior to phosphate release and a slower step prior to ADP release.

Author contributions: C.M.Y. designed research; D.V.T., J.M.M., A.M.S., and C.M.Y. performed research; D.V.T., J.M.M., J.P.D., D.D.T., and C.M.Y. contributed new reagents/analytic tools; D.V.T., J.M.M., and C.M.Y. analyzed data; and D.V.T., J.M.M., and C.M.Y. wrote the paper.

The authors declare no conflict of interest.

This article is a PNAS Direct Submission.

[1]To whom correspondence should be addressed. Email: cmy11@psu.edu.

This article contains supporting information online at www.pnas.org/lookup/suppl/doi:10.1073/pnas.1517566112/-/DCSupplemental.

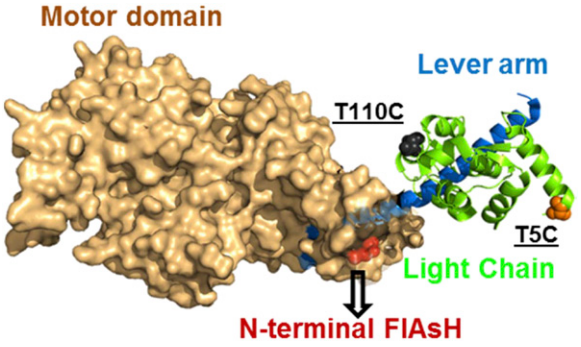

Fig. 1. Fluorescent probe location. The crystal structure of MV (PDB 1W7J) is shown with the probe locations. A tetracysteine motif (CCPGCC) was inserted at the N terminus which is depicted by labeling (red) the N-terminal residue (E5). Two labeling sites on calmodulin, T110C and T5C, are shown by labeling the corresponding residue in the essential light chain. T110C was labeled with QSY-9, and T5C was labeled with the QSY-9 or IAANS probe. FlAsH acted as a donor in the QSY-9–labeled T110C or T5C constructs and as an acceptor in the IAANS-labeled T5C construct.

occurs in two steps, with the first, fast step occurring before phosphate release. The slower power stroke step occurs before ADP release which is hypothesized to be a strain-sensitive step in the catalytic cycle of MV. Our work provides crucial insights into the structural details of lever arm swing in relation to the different steps in the catalytic cycle of myosin motors.

Results

Site-Specific Fluorescent Labeling. We have generated three constructs to determine the precise timing and kinetics of the lever arm swing. All three have a MV motor domain followed by a single IQ motif with an N-terminal tetracysteine site (referred to as "MV" throughout) that binds FlAsH, a bis-arscenical, fluorescein-based dye (MV-F) (Fig. 1). In one construct, calmodulin (CaM) containing a single cysteine at the N terminus (T5) was labeled with (2-(4'-(iodoacetamido)anilino)Naphthalene-6-sulfonic acid (IAANS) and exchanged onto MV (MV-F.IAANS). In another construct, CaM containing a single cysteine at the C terminus (T110) was labeled with the nonfluorescent acceptor QSY-9 and exchanged onto MV (MV-F.QSY). We also measured the recovery and power stroke with a construct that had QSY-labeled CaM at the T5C position (MV-F.QSY$_N$) (*SI Appendix*, Fig. S3). The labeling efficiency of FlAsH at the N-terminal site was nearly 100%, whereas that of IAANS was 67% at T5C and that of QSY was 75% at T110C and 82% at T5C. The efficiency of CaM exchange was nearly 100%. FlAsH was either excited directly (488 nm, FlAsH–QSY pair) or by FRET (365 nm, IAANS–FlAsH pair), and emitted fluorescence was measured with a 515-nm long-pass filter in the stopped-flow. The donor–acceptor pairs allowed us to examine the mechanism of lever arm swing during the formation of the pre- and postpower stroke states.

Functional Assays of Labeled MV. The maximum rate of actin-activated ATPase (k_{cat}) was similar for unlabeled and CaM-exchanged MV constructs and was slightly reduced (20–30%) for the FlAsH-labeled constructs (*SI Appendix*, Fig. S1 and Table S1). The actin dependence of the ATPase activity (K_{ATPase}) was unchanged by labeling in all constructs. The in vitro motility rates were similar in each construct (labeled and unlabeled; *SI Appendix*, Table S1) and were similar to values reported for wild-type MV 1IQ (7). Therefore, the fluorescence labeling strategy had a modest impact on ATPase activity and no significant impact on in vitro motility.

Lever Arm Swing During the Recovery Stroke. We measured the kinetics of lever arm swing during the transition from the postpower stroke (post-PS) to prepower stroke (pre-PS) states (i.e., during the recovery stroke) with the MV-F.IAANS and MV-F.QSY constructs. FlAsH fluorescence was monitored after mixing 0.25 μM dually labeled MV with different concentrations of ATP. We interpret our results in the context of Scheme 2, which consists of the formation of a collision complex (K_1) followed by a transition into the weak actin-affinity state (K_2) and then a priming of the active site for ATP hydrolysis (K_{3A}) and chemical hydrolysis (K_{3B}). We observed an increase in FlAsH fluorescence in the FlAsH–QSY pair, whereas with the IAANS–FlAsH pair we observed a decrease in FlAsH fluorescence (Fig. 2 *A* and *B*, *Inset*). The transients were best fit to a double exponential function. The fast and slow phases were plotted as a function of ATP concentration, and the fast phase was hyperbolically dependent on ATP concentration (Fig. 2) (see *SI Appendix*, Fig. S2 for single-turnover measurement). The amplitude of the slow phase was less than 10% of the total signal and was not characterized further (Fig. 2*C*). The rates of the fast phase were fit to a hyperbola to obtain the maximum rate of the fluorescence change which we modeled to be the recovery stroke rate constant (k_{+3A}), where k_{+2} is fast (~1,000·s^{-1}) and k_{-2} is very slow (8). The recovery stroke rate constant was similar in the FlAsH–QSY (330 ± 7·s^{-1}) and IAANS–FlAsH (312 ± 12·s^{-1}) donor–acceptor pairs (Fig. 2 *A* and *B*, respectively) and in the MV-F.QSY$_N$ construct (311 ± 11·s^{-1}) (*SI Appendix*, Fig. S3 *A* and *C*). The average rate of the slow phase was 8 ± 4·s^{-1} (FlAsH–QSY) and 9 ± 4·s^{-1} (IAANS–FlAsH). To compare the recovery stroke rate constant to the well-characterized intrinsic tryptophan fluoresce signal (8), we measured the rate of ATP binding to unlabeled MV in a separate experiment. We mixed 0.5 μM of unlabeled MV with different concentrations of ATP and measured the enhancement in tryptophan fluorescence (Fig. 2*A*). The data were fit to a single exponential function, and the rates were plotted as a function of ATP concentration. The fit of the data to a hyperbolic function allowed determination of the maximal rate of the fluorescence change and/or formation of the active site conformation that is competent for ATP hydrolysis (k_{+3A} = 332 ± 28·s^{-1}), which matches well with the recovery stroke rate constant. The results demonstrate that formation of the prepower stroke state (recovery stroke) is tightly coupled to formation of the hydrolysis competent state.

$$\underset{\text{Post-PS}}{\text{M+ATP}} \overset{K_1}{\Leftrightarrow} \underset{\text{Post-PS}}{\text{M(ATP)}} \overset{K_2}{\Leftrightarrow} \underset{\text{Post-PS}}{\textbf{M.ATP}} \overset{K_{3A}}{\Leftrightarrow} \underset{\text{Pre-PS}}{\textbf{M**.ATP}} \overset{K_{3B}}{\Leftrightarrow} \underset{\text{Pre-PS}}{\text{M**.ADP.Pi}}$$

Scheme 2. Kinetic steps associated with the myosin recovery stroke.

Lever Arm Swing During the Power Stroke. To measure the lever arm swing during the power stroke, a sequential mix, single-turnover setup was used. We mixed 0.15–0.25 μM of the dually labeled MV with 0.1–0.2 μM ATP which was held in the delay line for 10 s for hydrolysis to occur and then was mixed with different concentrations of actin. We found our results could be best interpreted in the context of Scheme 3. We observed a biphasic decrease in FlAsH fluorescence with the FlAsH–QSY pair and a biphasic increase with the IAANS–FlAsH pair (Fig. 3 *A* and *B*, *Insets*). The rate of the fast phase was actin dependent, whereas the slow phase was independent of the actin concentration. The amplitudes of both phases were dependent on actin concentration, with the fast phase dominant at higher actin concentrations (Fig. 3*C*). The rate of the fast phase was plotted as a function of actin concentration and fit to a hyperbolic function to determine the maximum rate of the fluorescence change or fast power stroke rate constant (k'_{+4A}). The rate constant of the fast power stroke was determined to be 352 ± 33·s^{-1} (FlAsH–QSY) or 493 ± 119·s^{-1} (IAANS–FlAsH), whereas the average slow power

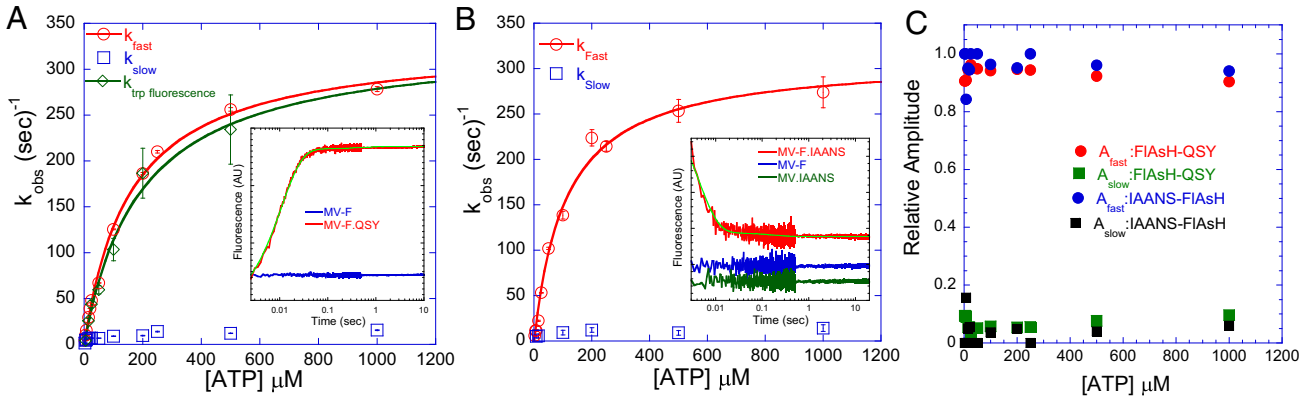

Fig. 2. Kinetics of the recovery stroke. (*A* and *B*) The kinetics of lever arm swing during the recovery stroke was measured by mixing 0.25 μM MV-F.QSY (*A*) or MV-F.IAANS (*B*) with different concentrations of ATP. A biphasic fluorescence increase (FlAsH–QSY pair with 500 μM ATP) (*A*, *Inset*) or a decrease (IAANS–FlAsH pair with 500 μM ATP) (*B*, *Inset*) was observed. The fast and slow phases are plotted as a function of ATP concentration, and the fast phase was fit to a hyperbola. The maximum rate of the fast phase was 330 ± 7·s^{-1} (MV-F.QSY) and 312 ± 12·s^{-1} (MV-F.IAANS). The observed rate of ATP-induced enhancement in tryptophan fluorescence in MV is plotted in *A* and fit to a hyperbola to determine the rate constant for the formation of the hydrolysis-competent state (332 ± 28·s^{-1}). Control traces of the respective donor-alone and acceptor-alone are also shown in the *Insets*. (*C*) The relative amplitudes of the fast and slow phases are plotted as a function of ATP concentration.

stroke rate constant was 18 ± 9·s^{-1} (FlAsH–QSY) or 20 ± 13·s^{-1} (IAANS–FlAsH). With the MV-F.QSY$_N$ construct, the rate constant of the fast power stroke was 290 ± 64·s^{-1}, and the rate constant of the slow power stroke was 12 ± 3·s^{-1} (*SI Appendix*, S3 *B* and *D*). To put the lever arm swing into an overall perspective of the catalytic cycle and to gain insights into the controversy regarding the precise timing of the swing, we measured the rate of phosphate release with the MV-F.QSY construct. The phosphate release rate constant was measured by monitoring the enhancement of fluorescence upon binding of phosphate to the phosphate-binding protein (PBP) covalently labeled with *N*-[2-(1-maleimidyl)ethyl]-7-(diethylamino)coumarin-3-carboxamide (MDCC-PBP) (Fig. 3*A*) and was found to be slower (k'_{+4B} = 201 ± 11·s^{-1}) than the fast power stroke and similar to previous studies (8–10). Thus, we provide evidence with three different donor–acceptor pairs that the power stroke occurs in two steps, a fast power stroke (k'_{+4A}) that occurs before phosphate release and a slower power stroke (k'_{+5A}) that occurs after phosphate release. We supported our experimental conclusions by performing simulations to compare the rate constants of lever arm swing and Pi release in two different kinetic models. In one model the lever arm swing occurs before Pi release (model 1; see rate constants in *SI Appendix*, Table S5), and in another model the swing occurs concurrent with Pi release (model 2, with k'_{+4} as a single step = 201·s^{-1}). The fits of the transients at 2.5 μM, 5 μM, 10 μM, and 20 μM actin are shown for model 1 (*SI Appendix*, Fig. S4), and fits at 2.5 μM and 20 μM are shown for model 2 (*SI Appendix*, Fig. S4, *Inset*). The transients fit well to model 1, in which the swing occurs before Pi release, but fit poorly to model 2.

$$\underset{\text{Pre-PS}}{\text{A+M**.ADP.Pi}} \overset{K_9}{\Leftrightarrow} \underset{\text{Pre-PS}}{\textbf{AM**ADP.Pi}} \overset{K'_{4A}}{\Leftrightarrow} \underset{\text{Intermediate}}{\textbf{AM*ADP.Pi}} \overset{K'_{4B}}{\Leftrightarrow} \underset{\text{Intermediate}}{\textbf{AM*ADP+Pi}} \overset{K'_{5A}}{\Leftrightarrow} \underset{\text{Post-PS}}{\textbf{AM.ADP}} \overset{K'_{5B}}{\Leftrightarrow} \underset{\text{Post-PS}}{\text{AM.ADP}} \overset{K'_{5C}}{\Leftrightarrow} \underset{\text{Post-PS}}{\text{AM+ADP}}$$

Scheme 3. Kinetic steps associated with the myosin power stroke.

Myosin binding to pyrene-labeled actin results in a fluorescence quenching that traditionally has been considered to measure a conformational change when myosin undergoes the transition from weak to strong actin binding (8). We measured the rate of quenching of pyrene fluorescence upon mixing of MV-F.ADP.Pi with different concentrations of pyrene actin (*SI Appendix*, Fig. S5). A sequential mix setup was used wherein MV-F was mixed with 10 μM ATP, held in the delay line for 1 s, and then mixed with different concentrations of pyrene-actin. A similar experiment was performed in which excess ADP (0.5 mM) was present in the final mix to ensure single-turnover conditions. A decrease in pyrene fluorescence was observed which was fit to a single exponential in the absence of ADP or a double exponential in the presence of ADP. The rate of the fast phase was hyperbolically dependent on the pyrene-actin concentration and reached a maximum rate of 32 ± 4·s^{-1}, which was similar to previously published work (8, 11). Although the structural change associated with the pyrene actin fluorescence signal has not been fully characterized (12, 13), this step is slower than the fast power stroke rate constant.

Lever Arm Swing During ADP Binding and Release. Although previous studies of MV have well characterized the kinetics of the actomyosin.ADP states (8, 9, 14), the movement of the lever arm during these steps is still unclear. Thus, we examined the FRET signal during ADP association and dissociation experiments and interpreted the results in the context of Scheme 3. To measure the rate of lever arm swing during ADP binding, the FRET signal was monitored after mixing acto-MV-F.QSY (0.25 μM MV; 0.5 μM actin) or acto-MV-F.IAANS (0.25 μM MV; 0.5 μM actin) with different concentrations of ADP. Upon ADP binding there was an increase in FlAsH fluorescence with the FlAsH–QSY construct (biphasic) and a decrease in the IAANS–FlAsH construct (*SI Appendix*, Fig. S6 *A* and *B*, *Insets*). The relative amplitudes of the ADP binding-induced change in FRET were much smaller (10–15%) than the ATP-induced change in FRET (*SI Appendix*, Fig. S6*C*). The fast phase was plotted as a function of ADP concentration and fit to a linear function, but the slow phase in MV-F.QSY was independent of ADP concentration (~4·s^{-1} and relative amplitude of 50%). The slope of the linear fit was determined to be 7.2 ± 0.6 μM^{-1}·s^{-1} (FlAsH–QSY; *SI Appendix*, Fig. S6*A*) and 7.8 ± 1.2 μM^{-1}·s^{-1} (IAANS–FlAsH; *SI Appendix*, Fig. S6*B*), which match well with the second-order rate constant for ADP binding to MV (k'_{-5C}) measured by other methods, such as flourescently labeled ADP (8, 9, 14). To measure the lever arm swing during the ADP release steps, a preequilibrated mixture of acto-MV-F.IAANS.ADP (0.5 μM actin, 0.25 μM MV, and 10 μM ADP) was mixed with KMg50 buffer (no chase). We observed an increase in FlAsH fluorescence that fit to a single exponential function (k_{obs} = 33 ± 5·s^{-1}), which is slower than predicted (~85·s^{-1}) based on k_{obs} being the sum of the association and dissociation reaction (14). This difference could be caused by off-pathway actomyosin.ADP states, which have been proposed (15). To measure the rate constant of ADP isomerization (k'_{+5B}) in

BIOCHEMISTRY

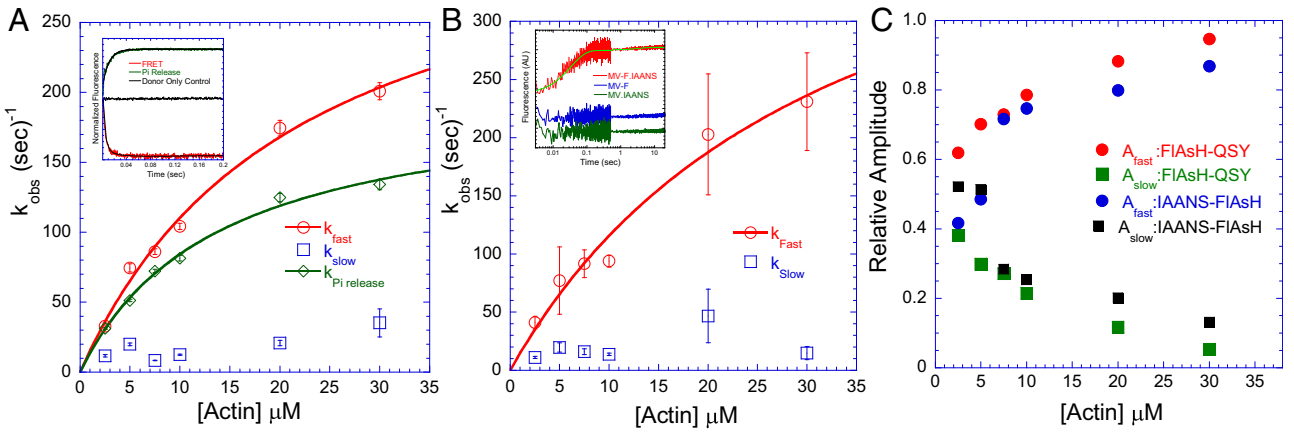

Fig. 3. Kinetics of the power stroke. The kinetics of lever arm swing during the power stroke were measured by sequential mix single-turnover experiments (final concentrations: 0.15–0.25 μM MV, 0.1–0.2 μM ATP, and varying actin concentrations). (*A*) In the MV-F.QSY construct we observed a biphasic decrease in FlAsH fluorescence [*Inset*: representative traces of the FRET signal (red, $k_{Fast} = 269 \pm 18 \cdot s^{-1}$) and phosphate release signal (green, $k_{obs} = 97 \pm 1 \cdot s^{-1}$) at 30 μM actin]. (*B*) In the MV-F.IAANS construct we observed a biphasic increase in FlAsH fluorescence (*Inset*: representative traces at 10 μM actin). In both constructs the observed rate of the fast phase increased as a function of actin concentration, but the slow phase remained unchanged. For the FlAsH–QSY construct in *A*, the maximum rate of the fast phase was $352 \pm 33 \cdot s^{-1}$, and the average rate of the slow phase was $18 \pm 9 \cdot s^{-1}$. For the IAANS–FlAsH construct in *B*, the maximum rate of the fast phase was $493 \pm 119 \cdot s^{-1}$, and the average rate of the slow phase was $20 \pm 13 \cdot s^{-1}$. The observed rate of phosphate release was also measured with the MV-F.QSY construct and was plotted as a function of actin concentration in *A* (same concentrations as above and 4.5 μM PBP). The hyperbolic fit of the data allowed determination of the phosphate release rate constant ($201 \pm 11 \cdot s^{-1}$). (*C*) The relative amplitudes of the fast and slow phases in the FRET signal were plotted as a function of actin concentration.

the dual-labeled construct, ADP release was measured with an ATP chase experiment. A preequilibrated mixture of acto-MV-F.QSY.ADP (0.5 μM actin, 0.25 μM MV, and 5 μM ADP) was mixed with 2 mM ATP. We observed a biphasic increase in the FlAsH fluorescence (*SI Appendix*, Fig. S6*A*, *Lower Inset*). A fast phase of $32 \pm 0.1 \cdot s^{-1}$ (k'_{+5C}) and a slow phase of $5.3 \pm 0.3 \cdot s^{-1}$ (k'_{+5B}) (with a relative amplitude of 96% of the fast phase) were observed. The slow phase corresponds well with the k_{cat} of the MV-F.QSY construct ($6.2 \pm 0.1 \cdot s^{-1}$), which we determined is the rate-limiting isomerization of the nucleotide binding pocket (14). Our overall interpretation of the kinetics of the structural changes associated with the actomyosin.ADP states is based on the sequential mix power stroke experiments and the ADP binding and dissociation experiments. We modeled the slow phase of the lever arm swing ($k'_{+5A} \sim 20 \cdot s^{-1}$) to be a step before the ADP isomerization step (k'_{+5B}) (14). We reasoned that because the slow power stroke is threefold faster than the ADP-isomerization step, the slow power stroke must occur before the isomerization.

Structural States of the Lever Arm Monitored with Time-Resolved FRET. We determined the distribution of structural states under equilibrium conditions detected by time-resolved (TR) FRET between the FlAsH–QSY probe pair. The mole fraction that participated in FRET was 0.66, which is consistent with the fraction of CaM labeled with QSY (0.75). The global analysis of the TR-FRET data fit well to a model described in *SI Appendix*, *Supplemental Methods* in which there are two structural states, the prepower stroke state with a longer distance (66 ± 2 Å), and a postpower stroke state with a shorter distance (37 ± 9 Å) (*SI Appendix*, Figs. S7–S10 and Table S2). The postpower stroke state demonstrated a wider distance distribution, suggesting that the lever arm is more dynamic in this state (Fig. 4). In the presence of saturating ATP (1 mM) the mole fraction of the prepower stroke state was favored (0.575 compared with 0.425 for the postpower stroke). The calculated equilibrium constant between the pre- and postpower stroke states in the presence of ATP ($K_{eq} = 1.35$) was similar to that measured by rapid quench studies (8). In contrast, in the absence of nucleotide (Apo) and in the presence of ADP the postpower stroke state was favored, especially in the presence of actin (nearly 100% postpower stroke in rigor and ADP). There is no crystal structure of MV in the prepower stroke state, but we generated a structural model by aligning the Apo MV structure (16) and the prepower stroke structure of smooth muscle myosin in the presence of ADP.BeF_X (*SI Appendix*, Fig. S11) (17). We found that the predicted distance change in the probe positions between the Apo and prepower stroke states (27 Å) was similar to the distance change we determined by FRET (20 Å). A previous FRET study examined the distance between a probe on the regulatory light chain and another probe near the nucleotide-binding pocket in *Dictyostelium* myosin II and found evidence for three nucleotide-dependent conformations of the lever arm, but these results were fit to a discrete distance model (reported distances of 20, 43, and 79 Å) instead of to a distance distribution model (18). It is possible that changes in probe orientation could account for the observed FRET changes, especially with the N-terminal FlAsH probe which is bifunctionally bound to the tetracysteine site. However, our measurements of time-resolved fluorescence anisotropy (*SI Appendix*, Tables S3 and S4) showed that the probe dynamics do not change with actin or nucleotide binding; thus the changes in FRET and the detected distance distributions likely reflect changes in

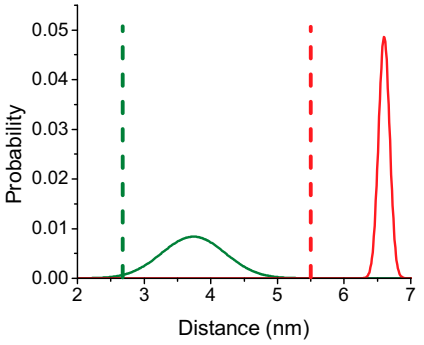

Fig. 4. Interprobe distances measured by TR-FRET. Postpower stroke (green) and prepower stroke (red) distances and distance distributions measured by TR-FRET (solid lines) in the MV-F.QSY construct (*SI Appendix*, Table S2). Dotted lines correspond to the distances determined in the crystal structure of the pre- and postpower stroke states, respectively, as shown in *SI Appendix*, Fig. S11.

interprobe distance and not in probe orientation. Although the distance changes observed could result from changes in the N-terminal region, we favor the interpretation that our results reflect movement of the light chain-binding region without major rearrangements of the N-terminal region. However, structural changes in the N-terminal region have been reported in different myosins. A recent crystal structure of myosin VI demonstrates that the N-terminal region forms important interactions with the converter to stabilize the position of the lever arm (19). In addition, a structure of myosin Ib demonstrates that an N-terminal extension makes contact with the lever arm helix and stabilizes the postpower stroke state; however, this extension is not present in MV (20). There is little evidence of major structural changes in the N-terminal region of MV as a function of nucleotide state, and examination of the flexibility of the region with computation modeling found similar rmsd values for the ADP (1W7I, 5.27 Å), ADP-BeF_X (1W7J, 4.71 Å), and Apo (1OE9, 6.78 Å) (the Protein Data Bank ID code and rmds are given in parentheses, respectively, for each structure) (11).

Discussion

ATP binding followed by hydrolysis and the subsequent actin-activated product release drives a reversible movement of the lever arm region in myosin motors. For decades researchers have investigated the temporal kinetics of how structural changes in myosin and force generation are correlated with the product release steps (2, 5). Before this study, a number of investigators attempted to measure the kinetics of lever arm swing in solution studies by using indirect methods. Monitoring the conformation of the relay helix, a structural element that couples the nucleotide binding and the lever arm regions, has been a method of choice. Either by monitoring the fluorescence of a conserved tryptophan at the distal end of relay helix (21, 22) or by using strategically placed FRET probes (23–25), the bent and straight conformation of the relay helix has been correlated to the pre- and postpower stroke states of the lever arm, respectively. We measured the structural kinetics of the lever arm swing directly in comparison with the rates of ATP binding and product release by using three donor–acceptor pairs in an MV construct. We circumvented the use of any nonnative fluorescent fusion proteins and used chromophore-labeled CaM bound to the lever arm domain.

Recovery Stroke. Studies based on transient TR-FRET of the relay helix have shown that the recovery stroke occurs after ATP binding (24). We demonstrate that the lever arm swings from the postpower stroke to the prepower stroke state upon formation of the hydrolysis-competent state (k_{+3A}) (shown in bold in Scheme 2). The rate of formation of the hydrolysis-competent state monitored by enhancement of tryptophan fluorescence closely matches the maximal rate of lever arm swing during the recovery stroke. The rate constants determined from the tryptophan fluorescence signal and chemical hydrolysis were found to be similar in MV (8), suggesting that this signal monitors the formation of the hydrolysis-competent state. The TR-FRET studies demonstrate that the lever arm populates a wider distribution of distances in the postpower stroke state than in the prepower stroke state (23, 25); these results are similar to those of the structural studies of the relay helix and suggest structural coupling between the relay helix and lever arm. Our results support the conclusion that the recovery stroke occurs at the same rate as the conformational change in the relay helix that precedes ATP hydrolysis. Thus, the recovery stroke is associated with the priming of the switch elements into a closed state for efficient hydrolysis of the ATP molecule.

Power Stroke. We measured the kinetics of the primary force-generating steps of the actomyosin ATPase cycle with our system and compared it to the rate of actin-activated phosphate release. The maximal rate constant of the fast phase of lever arm swing with both constructs (MV-F.IAANS = 493 ± 119·s^{-1} and MV-F.QSY = 352 ± 33·s^{-1}) was faster than the Pi release rate constant (MV-F.QSY = 201 ± 11·s^{-1}). This result demonstrates that the lever arm swings to generate force after actin binding and before Pi release. During this first step of the power stroke (K'_{4A}), the lever arm transitions from a prepower stroke state to an intermediate state (shown in bold in Scheme 3). A similar conclusion was obtained by measuring the bent-to-straight position of the relay helix in *Dictyostelium* myosin II, although the intermediate state was not observed (23). Therefore, the results suggest that the movement of the relay helix and the lever arm are closely coupled during the power stroke. Several studies based on muscle fiber or myofibril mechanics suggest a model wherein the force-generation step precedes the release of Pi from the active site (26–30). Alternatively, Llinas et al. (19) recently reported a crystal structure of myosin VI that contains Pi in the back-door tunnel while the lever arm is in a prepower stroke state. However, it is possible that the power stroke occurs when Pi is still in the tunnel, but the actual release of phosphate into solution is slower. Single-molecule studies have provided significant insight into the force-generating mechanism. Although it is difficult to measure the working stroke and Pi release simultaneously in a single-molecule setup (31), a study by Capitanio et al. (32) provides enhanced time resolution. The results suggest that the working stroke occurs within an interval of 2 ms after the initial binding of skeletal muscle myosin to actin. This study provides evidence of a fast power stroke that may precede Pi release, because in skeletal muscle myosin Pi release is relatively slow [50–100·s^{-1} at 25 °C and low ionic strength (33, 34)]. There have been reports based on single-molecule studies that demonstrate the reversibility of the power stroke and actomyosin detachment in the presence of high Pi concentrations and load (35, 36). Takagi et al. (30) concluded the power stroke occurs before Pi release because in the presence of an isometric force clamp only shorter events (20–40 ms) were sensitive to power stroke reversal induced by Pi binding and load. A study by Debold et al. (36) proposes a model in which the power stroke is completed before Pi release and Pi can bind to the AM.ADP state and dissociate it from actin. Overall, our results support a model in which the lever arm swing plays a role in gating Pi release, as is consistent with the hypothesis that actin dramatically accelerates the rate of lever arm swing and thus Pi release. If we assume that the power stroke gates Pi release in the absence of actin and that this step is rate-limiting, then the actin-induced acceleration is ∼20,000-fold. Different isoforms of myosins may have fine-tuned the rate of this force-generating swing, which regulates the release of Pi and in turn provides the characteristic functional property inherent to the isoform. Although our data are consistent with the hypothesis that the lever arm swing gates Pi release, it is likely that another conformational change after the fast power stroke limits Pi release. Our kinetic simulations are best fit by a model (shown in bold in Scheme 3) in which the lever arm swing precedes Pi release (*SI Appendix*, Fig. S4), but because the rate constants differ by less than a factor of two, the rate constants observed at lower actin concentrations are fairly similar.

Power Stroke Associated with the Actomyosin.ADP States. We observe a biphasic change in fluorescence during the lever arm swing upon actin-activated product release with all constructs. Following a fast swing of the lever arm and after Pi release, a slower conformational change (MV-F.IAANS = 20 ± 13·s^{-1} and MV-F.QSY = 18 ± 9·s^{-1}) was observed. We propose that these rates are associated with a transition from an intermediate to a postpower stroke lever arm during the transition between actomyosin.ADP states (shown in bold in Scheme 3). As hypothesized by Sleep and Hutton (37), a conformational state exists in the catalytic cycle of myosin which is found after Pi release but before ADP release (AM*ADP), and this state is not populated upon adding ADP to the rigor complex (37). We have previously shown that the transition from the strongly to weakly bound actomyosin.ADP state (ADP-isomerization or k'_{5B}) is the rate-limiting step of the ATPase cycle of MV (14). The rate of the lever arm swing that we observe here with

all constructs is faster than the ADP isomerization (k'_{5B}). This finding suggests that the actomyosin.ADP-associated swing of the lever arm occurs (k'_{5A}) before the ADP isomerization. The biphasic power stroke has been reported earlier in single-molecule studies of myosins I, II, and V (38, 39). Veigel et al. (40) propose a model wherein a 5-nm working stroke occurs in dimeric MV in the actomyosin.ADP states and that this stroke acts as a gate to relieve the strain that is generated by the binding of both heads to the actin filament. The second swing of the lever arm associated with the actomyosin.ADP state is hypothesized to be strain sensitive (41) and may alter the release rates of ADP from the nucleotide-binding pocket. We observed a relatively small fluorescence change during the ADP association and dissociation experiments (*SI Appendix*, Fig. S6) suggesting only small structural changes in the lever arm during these biochemical steps (K_{5B} and K_{5C}); this observation agrees well with our TR-FRET results (*SI Appendix*, Table S2). We have developed a model of the key conformational changes in the actomyosin ATPase cycle based on the available biochemical and structural data (*SI Appendix*, Fig. S12). MV complexed with ADP and Pi binds actin in the weak-binding state; this binding is followed by a rapid conformational change in the actin-binding region to allow attachment to actin (K_9) (11). Formation of the actomyosin complex leads to the rapid first step of the working stroke (K'_{4A}) followed by Pi release (K'_{4B}). The lever arm then undergoes a second swing (K'_{5A}) followed by the ADP isomerization (K'_{5B}) and an eventual release of ADP (K'_{5C}).

Conclusions

We demonstrate that actin activates a rapid movement of the lever arm (the myosin power stroke) before Pi release, providing evidence about the coordination of Pi release and force generation which has been a major controversy in the field of actomyosin-based motility for many years. Our results fit in well with proposed models that suggest actin binding enhances the rate of the lever arm swing, which kinetically drives the flux of myosin through a productive force-generating pathway as opposed to a futile cycle (5). Additional studies are necessary to assess the structural details of the allosteric pathway associated with actin activation of lever arm movement. Our results also are consistent with a model in which one directional motion is driven by alternating mechanical and chemical steps (30). In this model the chemical step provides the thermodynamic driving force which is gated by the preceding conformational change. In future studies it will be important to address how external load impacts the coordination between the lever arm swing and other steps in the myosin catalytic cycle.

Methods

Expression, purification, and labeling of MV were performed as described previously (42, 43). Additional information on methods is provided in *SI Appendix, Supplemental Methods*.

ACKNOWLEDGMENTS. We thank William Unrath for outstanding technical assistance. These studies were supported in part by NIH Grant AR032961 (to D.D.T.) and American Heart Association Grants 14SDG20480032 (to J.M.M.), 12PRE12050118 (to D.V.T.), and 14GRNT20380068 (to C.M.Y.).

1. Sellers JR (2000) Myosins: A diverse superfamily. *Biochim Biophys Acta* 1496(1):3–22.
2. Sweeney HL, Houdusse A (2010) Structural and functional insights into the Myosin motor mechanism. *Annu Rev Biophys* 39:539–557.
3. Huxley HE (1990) Sliding filaments and molecular motile systems. *J Biol Chem* 265(15): 8347–8350.
4. Holmes KC (1997) The swinging lever-arm hypothesis of muscle contraction. *Curr Biol* 7(2):R112–R118.
5. Málnási-Csizmadia A, Kovács M (2010) Emerging complex pathways of the actomyosin powerstroke. *Trends Biochem Sci* 35(12):684–690.
6. De La Cruz EM, Ostap EM (2004) Relating biochemistry and function in the myosin superfamily. *Curr Opin Cell Biol* 16(1):61–67.
7. Sun M, et al. (2006) Dynamics of the upper 50-kDa domain of myosin V examined with fluorescence resonance energy transfer. *J Biol Chem* 281(9):5711–5717.
8. De La Cruz EM, Wells AL, Rosenfeld SS, Ostap EM, Sweeney HL (1999) The kinetic mechanism of myosin V. *Proc Natl Acad Sci USA* 96(24):13726–13731.
9. Rosenfeld SS, Sweeney HL (2004) A model of myosin V processivity. *J Biol Chem* 279(38):40100–40111.
10. Yengo CM, Sweeney HL (2004) Functional role of loop 2 in myosin V. *Biochemistry* 43(9): 2605–2612.
11. Sun M, Rose MB, Ananthanarayanan SK, Jacobs DJ, Yengo CM (2008) Characterization of the pre-force-generation state in the actomyosin cross-bridge cycle. *Proc Natl Acad Sci USA* 105(25):8631–8636.
12. Taylor EW (1991) Kinetic studies on the association and dissociation of myosin subfragment 1 and actin. *J Biol Chem* 266(1):294–302.
13. Adamek N, Geeves MA (2014) Use of pyrene-labelled actin to probe actin-myosin interactions: Kinetic and equilibrium studies. *EXS* 105:87–104.
14. Jacobs DJ, Trivedi D, David C, Yengo CM (2011) Kinetics and thermodynamics of the rate-limiting conformational change in the actomyosin V mechanochemical cycle. *J Mol Biol* 407(5):716–730.
15. Hannemann DE, Cao W, Olivares AO, Robblee JP, De La Cruz EM (2005) Magnesium, ADP, and actin binding linkage of myosin V: Evidence for multiple myosin V-ADP and actomyosin V-ADP states. *Biochemistry* 44(24):8826–8840.
16. Coureux PD, et al. (2003) A structural state of the myosin V motor without bound nucleotide. *Nature* 425(6956):419–423.
17. Dominguez R, Freyzon Y, Trybus KM, Cohen C (1998) Crystal structure of a vertebrate smooth muscle myosin motor domain and its complex with the essential light chain: Visualization of the pre-power stroke state. *Cell* 94(5):559–571.
18. Shih WM, Gryczynski Z, Lakowicz JR, Spudich JA (2000) A FRET-based sensor reveals large ATP hydrolysis-induced conformational changes and three distinct states of the molecular motor myosin. *Cell* 102(5):683–694.
19. Llinas P, et al. (2015) How actin initiates the motor activity of Myosin. *Dev Cell* 33(4):401–412.
20. Shuman H, et al. (2014) A vertebrate myosin-I structure reveals unique insights into myosin mechanochemical tuning. *Proc Natl Acad Sci USA* 111(6):2116–2121.
21. Conibear PB, Málnási-Csizmadia A, Bagshaw CR (2004) The effect of F-actin on the relay helix position of myosin II, as revealed by tryptophan fluorescence, and its implications for mechanochemical coupling. *Biochemistry* 43(49):15404–15417.
22. Málnási-Csizmadia A, Woolley RJ, Bagshaw CR (2000) Resolution of conformational states of Dictyostelium myosin II motor domain using tryptophan (W501) mutants: Implications for the open-closed transition identified by crystallography. *Biochemistry* 39(51):16135–16146.
23. Muretta JM, Petersen KJ, Thomas DD (2013) Direct real-time detection of the actin-activated power stroke within the myosin catalytic domain. *Proc Natl Acad Sci USA* 110(18):7211–7216.
24. Nesmelov YE, et al. (2011) Structural kinetics of myosin by transient time-resolved FRET. *Proc Natl Acad Sci USA* 108(5):1891–1896.
25. Agafonov RV, et al. (2009) Structural dynamics of the myosin relay helix by time-resolved EPR and FRET. *Proc Natl Acad Sci USA* 106(51):21625–21630.
26. Dantzig JA, Goldman YE, Millar NC, Lacktis J, Homsher E (1992) Reversal of the cross-bridge force-generating transition by photogeneration of phosphate in rabbit psoas muscle fibres. *J Physiol* 451:247–278.
27. Kawai M, Halvorson HR (1991) Two step mechanism of phosphate release and the mechanism of force generation in chemically skinned fibers of rabbit psoas muscle. *Biophys J* 59(2):329–342.
28. Sleep J, Irving M, Burton K (2005) The ATP hydrolysis and phosphate release steps control the time course of force development in rabbit skeletal muscle. *J Physiol* 563(Pt 3):671–687.
29. Tesi C, Colomo F, Piroddi N, Poggesi C (2002) Characterization of the cross-bridge force-generating step using inorganic phosphate and BDM in myofibrils from rabbit skeletal muscles. *J Physiol* 541(Pt 1):187–199.
30. Takagi Y, Shuman H, Goldman YE (2004) Coupling between phosphate release and force generation in muscle actomyosin. *Philos Trans R Soc Lond B Biol Sci* 359(1452):1913–1920.
31. Capitanio M, et al. (2006) Two independent mechanical events in the interaction cycle of skeletal muscle myosin with actin. *Proc Natl Acad Sci USA* 103(1):87–92.
32. Capitanio M, et al. (2012) Ultrafast force-clamp spectroscopy of single molecules reveals load dependence of myosin working stroke. *Nat Methods* 9(10):1013–1019.
33. White HD, Belknap B, Webb MR (1997) Kinetics of nucleoside triphosphate cleavage and phosphate release steps by associated rabbit skeletal actomyosin, measured using a novel fluorescent probe for phosphate. *Biochemistry* 36(39):11828–11836.
34. Shaw MA, Ostap EM, Goldman YE (2003) Mechanism of inhibition of skeletal muscle actomyosin by N-benzyl-p-toluenesulfonamide. *Biochemistry* 42(20):6128–6135.
35. Sellers JR, Veigel C (2010) Direct observation of the myosin-Va power stroke and its reversal. *Nat Struct Mol Biol* 17(5):590–595.
36. Debold EP, Walcott S, Woodward M, Turner MA (2013) Direct observation of phosphate inhibiting the force-generating capacity of a miniensemble of Myosin molecules. *Biophys J* 105(10):2374–2384.
37. Sleep JA, Hutton RL (1980) Exchange between inorganic phosphate and adenosine 5′-triphosphate in the medium by actomyosin subfragment 1. *Biochemistry* 19(7):1276–1283.
38. Veigel C, et al. (1999) The motor protein myosin-I produces its working stroke in two steps. *Nature* 398(6727):530–533.
39. Veigel C, Molloy JE, Schmitz S, Kendrick-Jones J (2003) Load-dependent kinetics of force production by smooth muscle myosin measured with optical tweezers. *Nat Cell Biol* 5(11):980–986.
40. Veigel C, Wang F, Bartoo ML, Sellers JR, Molloy JE (2002) The gated gait of the processive molecular motor, myosin V. *Nat Cell Biol* 4(1):59–65.
41. Nyitrai M, Geeves MA (2004) Adenosine diphosphate and strain sensitivity in myosin motors. *Philos Trans R Soc Lond B Biol Sci* 359(1452):1867–1877.
42. Trivedi DV, David C, Jacobs DJ, Yengo CM (2012) Switch II mutants reveal coupling between the nucleotide- and actin-binding regions in myosin V. *Biophys J* 102(11):2545–2555.
43. Trivedi DV, Muretta JM, Swenson AM, Thomas DD, Yengo CM (2013) Magnesium impacts myosin V motor activity by altering key conformational changes in the mechanochemical cycle. *Biochemistry* 52(27):4710–4722.